Looking for magnetic monopoles at LHC with diphoton events

Luis N. Epele[a], Huner Fanchiotti[a], Carlos A. García Canal[a], Vasiliki A. Mitsou[b] and Vicente Vento[b,c]

[(a)] *Laboratorio de Física Teórica, Departamento de Física, IFLP, CONICET, Facultad de Ciencias Exactas, Universidad Nacional de La Plata C.C. 67, 1900 La Plata, Argentina.*
(E-mail: epele@fisica.unlp.edu.ar, huner@fisica.unlp.edu.ar, garcia@fisica.unlp.edu.ar)

[(b)] *Instituto de Física Corpuscular Universidad de Valencia and CSIC Apartado de Correos 22085, E-46071 Valencia, Spain.*
(E-mail: vasiliki.mitsou@ific.uv.es)

[(c)] *Departamento de Física Teórica Universidad de Valencia E-46100 Burjassot (Valencia), Spain.*
(E-mail: vicente.vento@uv.es)

Abstract

Magnetic monopoles have been a subject of interest since Dirac established the relation between the existence of monopoles and charge quantization. The intense experimental search carried thus far has not met with success. The Large Hadron Collider is reaching energies never achieved before allowing the search for exotic particles in the TeV mass range. In a continuing effort to discover these rare particles we propose here other ways to detect them. We study the observability of monopoles and monopolium, a monopole-antimonopole bound state, at the Large Hadron Collider in the $\gamma\,\gamma$ channel for monopole masses in the range 500–1000 GeV. We conclude that LHC is an ideal machine to discover monopoles with masses below 1 TeV at present running energies and with 5 fb^{-1} of integrated luminosity.

Pacs: 14.80.Hv, 95.30.Cq, 98.70.-f, 98.80.-k
Keywords: Quantum electrodynamics, duality, monopoles, monopolium, photon, proton.

1 Introduction

The theoretical justification for the existence of classical magnetic poles, hereafter called monopoles, is that they add symmetry to Maxwell's equations and explain charge quantization [1,2]. Dirac showed that the mere existence of a monopole in the universe could offer an explanation of the discrete nature of the electric charge. His analysis leads to the Dirac Quantization Condition (DQC),

$$e\,g = \frac{N}{2}\ ,\ \mathrm{N} = 1,2,...\ , \tag{1}$$

where e is the electron charge, g the monopole magnetic charge and we use natural units $\hbar = c = 1$. In Dirac's formulation, monopoles are assumed to exist as point-like particles and quantum mechanical consistency conditions lead to Eq. (1), establishing the value of their magnetic charge. Their mass, m, is a parameter of the theory.

Monopoles and their experimental detection have been a subject of much study since many believe in Dirac's statement [1],

"...one would be surprised if Nature had made no use of it [the monopole]."

All experimental searches for magnetic monopoles up to now have met with failure [3–13]. These experiments have led to a lower mass limit in the range of 350 GeV. The lack of experimental confirmation has led many physicists to abandon the hope in their existence.

Although monopoles symmetrize Maxwell's equations in form, there is a numerical asymmetry arising from the DQC, namely that the basic magnetic charge is much larger than the smallest electric charge. This led Dirac himself in his 1931 paper [1] to state,

"... the attractive force between two one-quantum poles of opposite sign is $(137/2)^2 \approx 4692\frac{1}{4}$ *times that between the electron and the proton. This very large force may perhaps account for why the monopoles have never been separated."*

Inspired by this old idea of Dirac and Zeldovich [1, 14, 15], namely, that monopoles are not seen freely because they are confined by their strong magnetic forces forming a bound state called monopolium [16, 17], we proposed that monopolium, due to its bound state structure, might be easier to detect than free monopoles [18, 19].

The Large Hadron Collider (LHC), which entered last year in operation colliding 3.5-TeV protons, will probe the energy frontier opening possibilities for new physics including the discovery of magnetic monopoles either directly, a possibility contemplated long time ago [20, 21], and revisited frequently [5, 9, 22–26] or through the discovery of monopolium, as advocated in refs. [18, 19]. The direct observation is based on the

search for highly ionizing massive particles at the ATLAS [27] and CMS [28] detectors or at the MoEDAL experiment [29], which is designed to search precisely for such exotic states.

If instead of single monopoles (antimonopoles) we deal with monopole-antimonopole pairs, as is the case at LHC, we expect that due to the very strong interaction many of them annihilate into photons inside the detector, either directly or by forming a monopolium bound state which will also disintegrate producing photons. Therefore we are led to study the production of monopoles and monopolium at LHC by the mechanism of photon fusion and its subsequent decay into two photons [30, 31].

In the next section we describe the dynamics of monopoles and review the production of monopole-antimonopole pairs. Section 2 discusses the annihilation of the virtual monopole-antimonopole pair into photons. In section 3 we review the production of monopolium and study its annihilation into photons. In section 4 we describe how to incorporate the elementary processes into $p-p$ scattering. In section 6 we present our results in the context of the present running features of LHC and in the last section we draw conclusions of our studies.

2 Monopole dynamics

The theory of monopole interactions was initially formulated by Dirac [14] and later on developed in two different approaches by Schwinger [32] and Zwanziger [33]. The formalism of Schwinger can be cast in functional form as a field theory for monopole-electron interaction which is dual to Quantum Electrodynamics (QED) [34]. The monopoles are considered fermions and behave as electrons in QED with a large coupling constant as a result of the DQC. In this formulation the conventional photon field is Dirac string dependent. Due to the large coupling constant and the string dependence, perturbative treatments à la Feynman are in principle not well defined. However, non perturbative high energy treatments, like the eikonal approximation, have rendered well defined electron-monopole cross sections [34, 35]. For the case of monopole production at energies higher than their mass the above procedure is not applicable, and being the treatment non perturbative, there is no universally accepted prediction from field theory.

A different scheme to understand monopole interactions was proposed by Ginzburg and Schiller [23, 24]. Using standard electroweak theory in the one-loop approximation to lowest non-vanishing order they derived an effective theory with coupling,

$$g_{\mathit{eff}} = \frac{g\omega}{\sqrt{4\pi}m}, \tag{2}$$

where g is the monopole coupling, ω the photon energy of the vertex and m the monopole mass. Thus, for virtualities smaller than ω and $\omega << m$, one can derive an effective Heinsenberg-Euler type effective Lagrangian for the box diagram with a small

coupling [23]. However, one can always ask the question: what will happen at higher orders? How can one treat the divergencies? The authors argue that in this kinematical region general considerations like gauge invariance, threshold behavior, etc., together with the perturbative approach allows an effective theory analogous to standard QED in lowest non trivial order only.

Certainly their procedure is a conjecture that is meaningful from the point of view of effective theories. Effective theories are in general non renormalizable. Higher orders would require counter terms with unknown constants to be fitted by experiments. If their philosophy is accepted it corresponds Nature to prove it or disprove it.

The Ginzburg-Schiller prescription is only valid below the monopole production threshold, and as such not very powerful from the point of view of phenomenology, because virtual particles, very far off-shell, can be easily confused with other scenarios. A complementary idea was proposed in ref. [25] and is beautifully explained in the thesis of Mulhearn [7]. These authors realized that a monopole interacts with an electron like a (duality transformed) positron, and therefore the effective coupling for electron-monopole is simply βg, where β is the velocity of the monopole. In order to study monopole-antimonopole production processes (via Drell-Yan) they simply turned the diagram around, thus constructing an effective vertex with coupling βg (see Fig. 1).

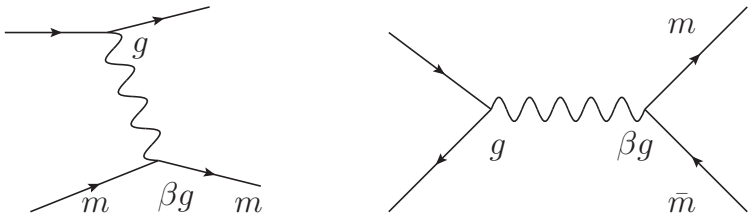

Figure 1: Elementary vertices of monopole-monopole and monopole-antimonopole photon coupling.

This scheme has been used to define an effective field theory to lowest order [25] which has been applied to Drell-Yan like monopole-antimonopole production [12, 25] and to monopole-antimonopole production by photon fusion [22, 26] (see Fig. 2).

Non perturbative solutions of field theories lead to momentum-dependent coupling constants and even momentum dependent masses. For example, the resolution of truncated Dyson-Schwinger equations leads to the freezing of the QCD running coupling (effective charge) in the infrared, which is best understood as a dynamical generation of a gluon mass function, giving rise to a momentum dependence which is free from infrared divergences [36]. These studies have motivated our starting hypothesis. We consider the diagrams of the Fig. 1 as the diagrams of an effective theory where

$$\alpha(q^2) \sim \beta(q^2) g, \tag{3}$$

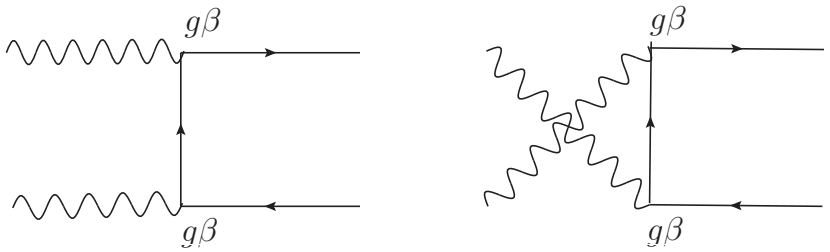

Figure 2: Elementary processes of monopole-antimonopole production via photon fusion.

and moreover, we assume, with Ginzburg and Schiller, that this effective theory is valid only to lowest non-vanishing order. The momentum dependence is probably much more involved, but we know of two instances where it reduces to βg, namely those of the figures. Effective theories, as it was said, are not renormalizable, and moreover higher orders in the field expansion will require additional counter terms and new constants to be fitted to the data, therefore our theory is at present only defined to lowest non-vanishing order. To construct the higher order approximation we should apply Weinberg's theorem [37] and construct all terms compatible with the symmetries. At present, and close to monopole-antimonopole threshold, we expect the lowest order term to be sufficient, for our purposes. Guided by simplicity and phenomenological inspiration we introduce an effective theory which is finite and well defined and we call this proposal the β *scheme*.

Note that the Ginzburg-Schiller scheme and the β scheme are in some sense complementary. The former is valid below the monopole threshold, while the latter above since β vanishes below threshold.

The aim here is to study possible signals of magnetic monopoles at LHC. According to previous studies [26], the most promising mechanism is photon fusion. The elementary diagrams contributing to pair production are those in Fig. 2, where the explicit couplings have been shown.

The photon-fusion elementary cross section is obtained from the well-known QED electron-positron pair creation cross section [38], simply changing the coupling constant ($e \to g\beta$) and the electron mass by the monopole mass $m_e \to m$, leading to

$$\sigma(\gamma\,\gamma \to m\overline{m}) = \frac{\pi\; g^4\,(1-\beta^2)\,\beta^4}{2\,m^2}\left(\frac{3-\beta^4}{2\beta}\log\left(\frac{1+\beta}{1-\beta}\right)-(2-\beta^2)\right), \qquad (4)$$

where β is the monopole velocity, a function of the center-of-mass energy, E. In Fig. 3 we show the $\omega = E/2\,m$ dependence of the adimensional functional form of Eq.(4) to show the effect of the $\beta\,g$ coupling. The solid curve corresponds to the electron-positron case, the dashed one to the monopole case which contains the β^4 factor. One should

notice the large effect associated with this factor in the vicinity of the threshold.

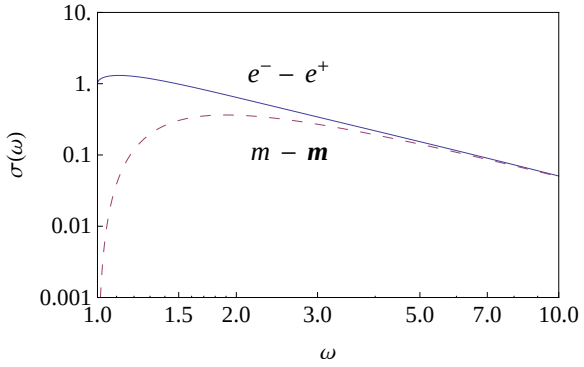

Figure 3: Adimensional functional form of the elementary photon-fusion cross section for electron-positron (solid) and that of the monopole-antimonopole (dashed) as a function of ω which shows the effect of the $\beta\, g$ coupling.

LHC detectors, apart from the MoEDAL experiment [29], have not been designed specifically to see monopoles directly and therefore even those which do not annihilate inside the detectors will be difficult to detect. However, the extreme sensitivity of LHC detectors to photons, due to the importance of the 2γ channel in detecting a low mass Higgs, makes them ideal for the purpose of detecting monopole-antimonopole annihilation.

The two photon process through monopole loops in the Ginzburg-Schiller scheme was studied already sometime ago both theoretically in ref. [23] and experimentally in ref. [5]. We have proceeded in this paper to perform the calculation in the β scheme.

3 Monopole-antimonopole annihilation into $\gamma\,\gamma$

It is natural to think that the enormous strength and long range of the monopole interaction leads to the annihilation of the pair into photons very close to the production point. Thus one should look for monopoles through their annihilation into highly energetic photons, a channel for which LHC detectors have been optimized.

In order to calculate the annihilation into photons we assume that our effective theory, a technically convenient modification of Ginzburg and Schiller's, agrees with QED at one loop order, and therefore we apply light-by-light scattering with the appropriate modifications as shown in Fig. 4. An interesting feature of the calculation is that the additional magnetic coupling will increase the cross section dramatically and therefore this measurement should lead to a strong restriction on the monopole mass. However, as we have seen, in $m-\overline{m}$ production, the large magnetic coupling is always multiplied

by the small electric one, leading to effective couplings $e\,g$, and the same will happen in detection. Thus, the effective coupling of the process is $e\,g$, and therefore has strengths similar to the strong interaction, not more.

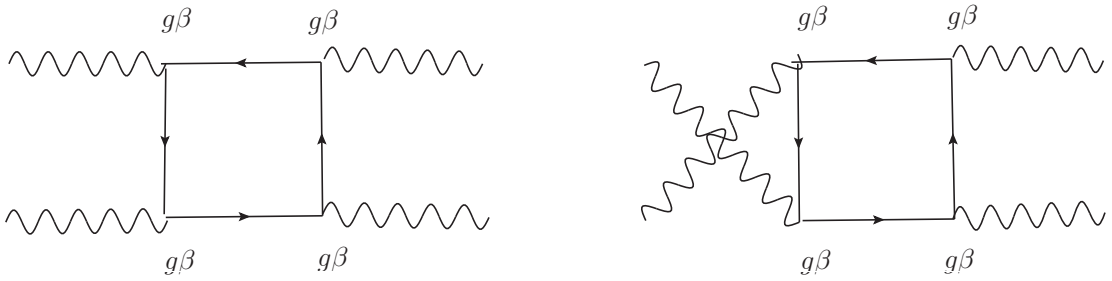

Figure 4: Elementary processes for monopole-antimonopole production and annihilation into photons.

Light-by-light scattering was studied by Karplus and Neuman [39, 40], who reproduced all previous low energy results by Euler [41] and high energy results by Achieser [42], and was later revisited and corrected by Csonka and Koelbig [43].

In the case of monopoles, with the appropriate changes, the expression for the cross section becomes,

$$\sigma_{\gamma\gamma}(\theta,\omega) = \frac{(g\beta)^8}{8\pi^2 m^2}\, X(\theta,\omega). \tag{5}$$

where $X(\omega)$ is $\frac{<|M|^2>}{\omega^2}$ in the notation of ref. [40]. In Fig. 5 we reproduce these results for forward scattering and right-angle scattering. In Fig. 6 (left) we show the ratio of the forward scattering to the right-angle cross sections and therefore show how the cross section, which is basically isotropic close to threshold, becomes anisotropic as the energy increases. In the same figure (right) we plot $X(\omega)$ for several values of ω as a function of angle. We note that the forward cross section is larger and the right-angle one smaller, than that for any other value of the scattering angle. As the energy increases the drop in the X function from $\theta = 0$ to $\pi/2$ increases.

It is clear from these figures that close to the threshold the cross section is quite isotropic and away from threshold the forward cross section, which is very difficult to measure, is much larger than the right-angle one. Since the detectors cannot detect all of the photons coming out, we take the right-angle cross section as a conservative indication of the magnitudes to be expected.

In Fig. 7 we show the effect of the β factor which diminishes greatly the cross section close to the monopole-antimonopole threshold.

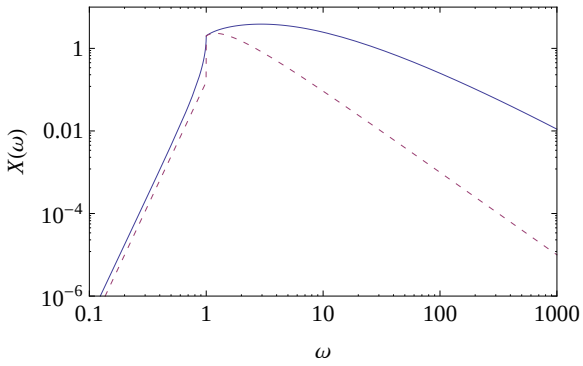

Figure 5: The light-by-light scattering quantity $X(\omega)$, which determines the cross section up to factors related to the coupling constant. The solid curve corresponds to forward scattering, the dashed one to right-angle scattering, both as a function of the dimensionless quantity ω.

4 Monopolium annihilation into $\gamma\,\gamma$

Recently we studied the production of monopolium by photon fusion at LHC [19]. The elementary subprocess calculated is shown in Fig. 8. The standard expression for the cross section of the elementary subprocess for producing a monopolium of mass M is given by

$$\sigma(2\gamma \to M) = \frac{4\pi}{E^2} \frac{M^2\,\Gamma(E)\,\Gamma_M}{\left(E^2 - M^2\right)^2 + M^2\,\Gamma_M^2}, \tag{6}$$

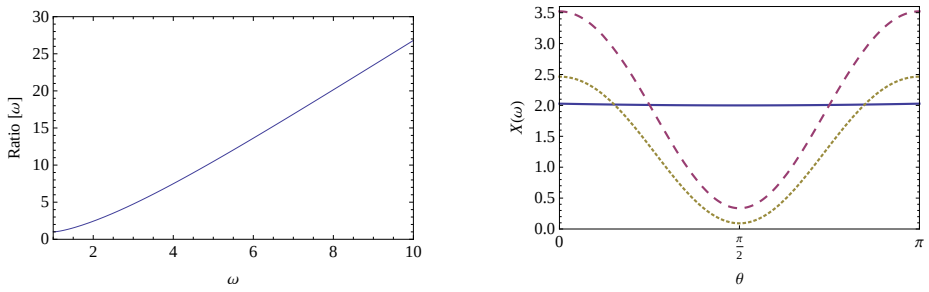

Figure 6: Left: ratio of the light-by-light scattering quantity $X(\omega)$ for forward to right-angle scattering as a function of ω. Right: angular dependence of the cross section for three values of ω (1 (solid) , 5 (dashed), 10 (dotted)) .

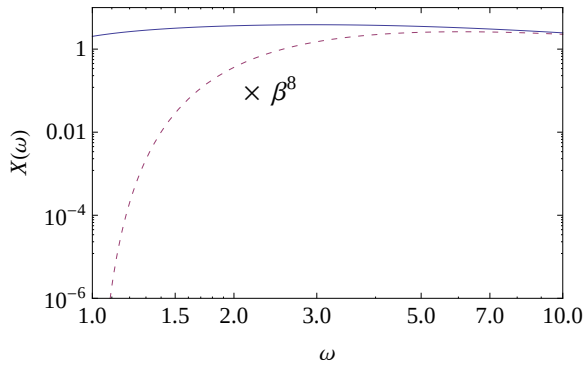

Figure 7: The effect of the β factor as a function of ω. The solid curve corresponds to electron scattering, while the dashed curve corresponds to the monopole case.

where $\Gamma(E)$, with E off mass shell, describes the production cross section. Note that $\Gamma[M] = 0$. Γ_M arises from the softening of the delta function, $\delta(E^2 - M^2)$ and therefore is, in principle, independent of the production rate $\Gamma(E)$ and can be attributed to the beam width [44, 45].

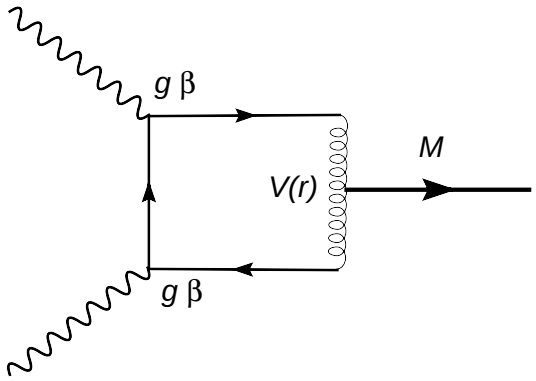

Figure 8: Diagrammatic description of the elementary subprocess of the monopolium production from photon fusion. $V(r)$ represents the interaction binding the monopole-antimonopole pair to form monopolium.

In Fig. 9 we show the total cross section for monopolium production from photon fusion under present LHC running conditions for a monopole mass (m) ranging from 500 to 1000 GeV. In the figure the binding energy is fixed for each mass (2 m/15), chosen so that for our case study, $m = 750$ GeV, the binding energy is 100 GeV and thus $M = 1400$ GeV. With this choice the monopolium mass (M) ranges from 933 to 1866 GeV. We notice that detection would be possible with an integrated luminosity of 5 fb^{-1} if the chosen binding energy is at the level of 10% of the monopole mass or

higher. In the present analysis we study binding energies small compared to the bound state mass, M, in order to be consistent with the formalism used.

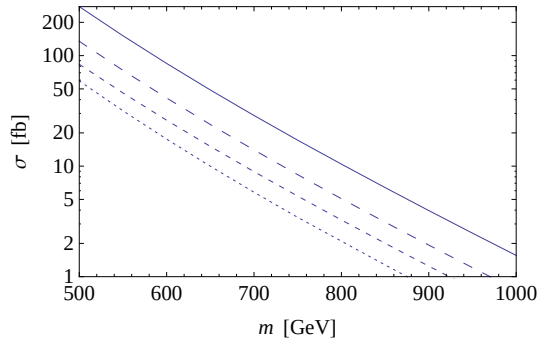

Figure 9: Total cross section for monopolium production at LHC with 3.5 TeV beams for monopole masses ranging from 500 to 1000 GeV (full curve). The broken curves represent the different contributions to the total cross section as described in the text: semi-elastic (dashed), elastic (short dashed) and inelastic (dotted). We have chosen a binding energy $\sim 2\,m/15$ and $\Gamma_M = 10$ GeV.

The interest in this paper is in the detection of photons after monopolium decay. The elementary subprocess is shown in Fig. 10, which could be considered as a contribution to light-by-light scattering in the presence of monopolium.

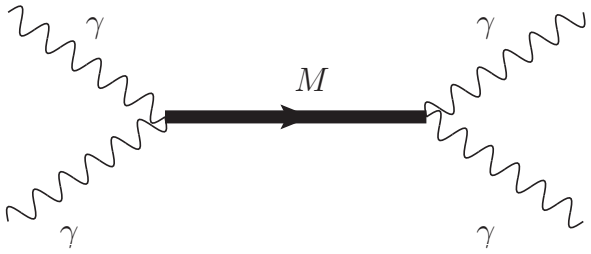

Figure 10: Diagrammatic description of the monopolium production and decay.

The standard expression for the cross section of this elementary subprocess, after having integrated over angles, is given by

$$\sigma(\gamma\,\gamma \to M \to \gamma\,\gamma) = \frac{4\pi}{E^2}\frac{M^2\,\Gamma^2(E)}{\left(E^2 - M^2\right)^2 + M^2\,\Gamma_M^2}. \tag{7}$$

Here $\Gamma(E)$, with E off mass shell, describes the vertex $\gamma\,\gamma\,M$. Monopolium is stable in the center of mass but we add an experimental Gaussian width $\Gamma_M \sim 10$ GeV in line with the values used in ref. [46].

We recall now the computation of the $\Gamma(E)$, which represents the vertex of the monopolium decay to $\gamma\,\gamma$. The calculation, following standard field-theory techniques of the decay of a non-relativistic bound state, leads to

$$\Gamma(E) = \frac{32\,\pi\,\alpha_g^2}{M^2}\,|\psi_M(0)|^2\,. \tag{8}$$

We have used the conventional approximations for this calculation: the monopole and antimonopole, forming the bound state, are treated as on-shell particles, when calculating the elementary scattering process shown on the right of Fig. 11; the bound state is described by a wave function obtained from a Coulomb-type interaction between the pair [19, 44, 45]. However, once the calculation is performed we substitute $2m$ by M, where m is the monopole mass to take into account binding. In the expression, α_g corresponds to the photon–monopole coupling and ψ_M is the monopolium ground state wave function.

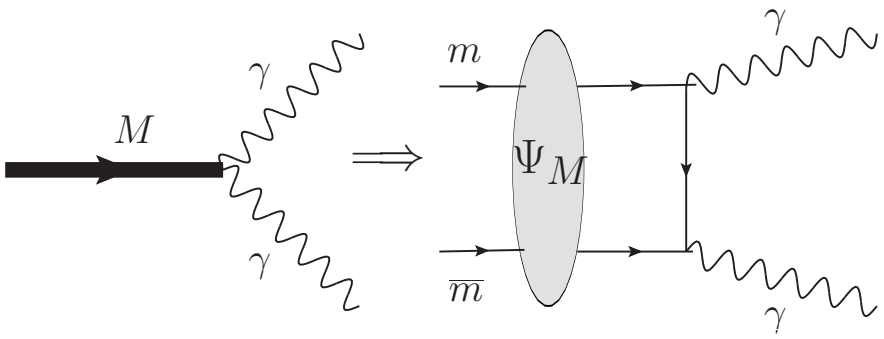

Figure 11: The monopolium vertex and its microscopic description .

Before we proceed let us raise a warning on our calculation. Bound relativistic systems are notoriously difficult dynamical objects. We proceed here by performing a non-relativistic calculation of the monopolium wave function. The validity of the non-relativistic approximation in the bound state wave functions was analyzed in a previous work [18]. In the dynamics of the decay formula the substitution of $2m$ by M constitutes an intuitive way to take the off-shellness of the monopoles, i.e. their binding energy in monopolium, into account. For the purposes of estimation both approximations seem reasonable specially since our binding energies will never exceed 15% of the monopole mass, i.e. less than 10% of the total mass of the system.

Using the Coulomb wave functions of ref. [18] expressed in the most convenient way to avoid details of the interaction, which will be parameterized by the binding energy, one has

$$|\psi_M(0)|^2 = \frac{1}{\pi}\left(2 - \frac{M}{m}\right)^{3/2}\; m^3, \tag{9}$$

and the effective monopole coupling theory described above in the case of monopolium production, gives rise to [19],

$$\frac{\Gamma(E)}{M} = 2\left(\frac{\beta^2}{\alpha}\right)^2 \left(\frac{m}{M}\right)^3 \left(2 - \frac{M}{m}\right)^{3/2}. \tag{10}$$

Here, α is the fine structure constant and β the monopolium velocity,

$$\beta = \sqrt{1 - \frac{M^2}{E^2}}, \tag{11}$$

which is the velocity of the monopoles moving in the monopolium system.

Note that due to the value of β the vertex vanishes at the monopolium mass, where the velocity is zero. Therefore a static monopolium is stable under this interaction. We refer to refs. [7, 25] for a thorough discussion on Lorentz invariance of the theory.

A caveat is due here. There is a duality of treatments in the above formulation as can be seen in Fig. 8. The static coupling is treated as a Coloumb like interaction of coupling g binding the monopoles into monopolium, although ultimately the details are eliminated in favor of the binding energy parameterized by the monopolium mass M. We find in this way a simple parametric description of the bound state. The dynamics of the production of the virtual monopoles, to be bound in monopolium, is described in accordance with the effective theory [25], and this coupling is βg. This is similar to what is done in heavy quark physics [47](see his figure 5), where the wave function is obtained by a parametric description using approximate strong dynamics while the coupling to photons is elementary.

The production cross section can now be written as,

$$M^2\, \sigma(\gamma\,\gamma \to M \to \gamma\,\gamma) = 16\,\pi \left(\frac{\beta}{\alpha}\right)^4 \left(\frac{m}{E}\right)^6 \left(2 - \frac{M}{m}\right)^3 \left(1 + \frac{M^2\Gamma_M^2}{E^4\beta^4}\right)^{-1}. \tag{12}$$

The above cross section satisfies comfortably the unitarity limit [48],

$$\sigma \leq \frac{\pi}{3E^2}. \tag{13}$$

To feel safe with our approximations we consider the binding energy much smaller than m, i.e. $M \sim 2m$. In this case the elementary cross section has two very different behaviors as shown in Fig. 12 : i) at threshold it is dominated by β and the cross section rises (see left figure); ii) away from threshold the dominant behavior is the $1/E$ dependence and the cross section drops faster than the unitary limit. The conflict between these two behaviors produces a wide bump-like structure.

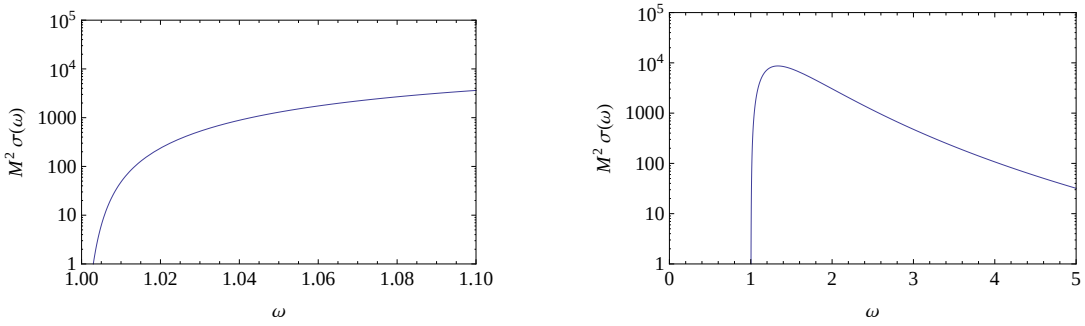

Figure 12: Elementary cross section as a function of $\omega = E/M$ in units of $1/M^2$ calculated for $m = 750$ GeV and $M = 1400$ GeV. Left: near threshold. Right: away from threshold.

5 Analysis of $p - p$ scattering

LHC is a proton-proton collider, therefore, in order to describe the production and desintegration of the monopole-antimonopole pair, we have to study the following processes above the monopole threshold ($\beta > 0 \rightarrow E \geq 2m$),

$$p + p \quad \rightarrow \quad p(X) + p(X) + \gamma + \gamma, \tag{14}$$

shown globally in Fig.13, where p represents the proton, X an unknown final state and we will assume that the blob is due exclusively to a) monopoles and b) monopolium. This diagram summarizes the three possible processes in each case:

a) monopole-antimonopole annihilation

i) inelastic $p + p \rightarrow X + X + \gamma + \gamma \rightarrow X + X + m + \overline{m} \rightarrow X + X + m + \overline{m} + \gamma + \gamma$

ii) semi-elastic $p + p \rightarrow p + X + \gamma + \gamma \rightarrow p + X + m + \overline{m} \rightarrow p + X + m + \overline{m} + \gamma + \gamma$

iii) elastic $p + p \rightarrow p + p + \gamma + \gamma \rightarrow p + p + m + \overline{m} \rightarrow\rightarrow X + X + m + \overline{m} + \gamma + \gamma$.

and

b) monopolium annhilation

i) inelastic $p + p \rightarrow X + X + \gamma + \gamma \rightarrow X + X + M \rightarrow X + X + M + \gamma + \gamma$

ii) semi-elastic $p + p \rightarrow p + X + \gamma + \gamma \rightarrow p + X + M \rightarrow p + X + M + \gamma + \gamma$

iii) elastic $p + p \rightarrow p + p + \gamma + \gamma \rightarrow p + p + M \rightarrow p + p + M + \gamma + \gamma$.

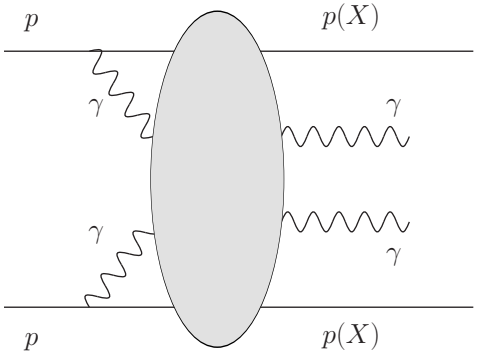

Figure 13: Processes contributing to the $\gamma\gamma$ cross section. The blob contains the three cases described in the text.

In the inelastic scattering, both intermediate photons are radiated from partons (quarks or antiquarks) in the colliding protons.

In the semi-elastic scattering one intermediate photon is radiated by a quark (or antiquark), as in the inelastic process, while the second photon is radiated from the other proton, coupling to the total proton charge and leaving a final state proton intact.

In the elastic scattering both intermediate photons are radiated from the interacting protons leaving both protons intact in the final state.

In the blob we incorporate in a) the elementary subprocess shown in Fig. 4 and described by Eq. (5) and in b) the elementary subprocess shown in Fig. 10 and described by Eq. (12).

We calculate $\gamma\gamma$ fusion for monopole-antimonopole and monopolium production following the formalism of Drees et al. [49].

In the inelastic scattering, $p+p \to X+X+(\gamma\gamma) \to X+X+(m+\overline{m})(\text{or } M)+\gamma+\gamma$, to approximate the quark distribution within the proton we use the Cteq6–1L parton distribution functions [50] and choose $Q^2 = \hat{s}/4$ throughout, where $\hat{s}$ is the center of mass energy of the elementary process.

We employ an equivalent–photon approximation for the photon spectrum of the intermediate quarks [51, 52].

In semi-elastic scattering, $p+p \to p+X+(\gamma\gamma) \to p+X+(m+\overline{m})(\text{or } M)+\gamma+\gamma$, the photon spectrum associated with the interacting proton must be altered from the equivalent–photon approximation for quarks to account for the proton structure. To accommodate the proton structure we use the modified equivalent–photon approximation of [49].

The total cross section is obtained as a sum of the three processes. The explicit expressions for the different contributions can be found in [26].

In order to obtain the differential photon-photon cross section from the above formalism we develop a procedure which we exemplify with the elastic scattering case. In

that case the pp cross section is given by [49, 53],

$$\sigma_{pp}(s) = \int_{s_{th}/s}^{1} dz_1 \int_{s_{th}/sz_1}^{1} dz_2 f(z_1) f(z_2) \sigma_{\gamma\gamma}(z_1 z_2 s), \tag{15}$$

where $\sqrt{s_{th}} = 2m$ (or M) is the threshold center of mass energy, $\sqrt{s}$ is the center of mass energy of the pp system and the f's represent the elastic photon spectrum.

We perform the following change of variables

$$v = z_1 z_2 \ , \ w = z_2 \ ,$$

which leads to

$$\sigma_{pp}(s) = \int_{s_{th}/s}^{1} dv \int_{v}^{1} \frac{dw}{w} f(\frac{v}{w}) f(w) \sigma_{\gamma\gamma}(vs). \tag{16}$$

Note that to fix the center of mass energy of the photons is equivalent to fix v. For fixed v we have,

$$\frac{d\sigma_{pp}}{dv}(s) = \int_{v}^{1} \frac{dw}{w} f(\frac{v}{w}) f(w) \sigma_{\gamma\gamma}(vs), \tag{17}$$

which can be rewritten in terms of E_γ, the center of mass energy of the photons, and the elementary photon-photon cross section as,

$$\frac{d\sigma_{pp}}{dE}(E_\gamma) = \frac{2E_\gamma}{s} \ \sigma_{\gamma\gamma}(s_{\gamma\gamma}) \ \int_{s_{\gamma\gamma}/s}^{1} \frac{dw}{w} f(\frac{s_{\gamma\gamma}}{w}) f(w). \tag{18}$$

This procedure can be generalized easily to the semi-elastic and inelastic cases, where the appropriate change of variables are

$$v = z_1 z_2 x_1 \ , \ w = z_2 x_1 \ , \ u = x_1$$

and

$$v = z_1 z_2 x_1 x_2 \ , \ w = z_2 x_1 x_2 \ , \ u = x_1 x_2 \ , \ t = x_2,$$

respectively which one has to introduce into integral expressions with a product of three f's (semi-elastic) or four f's (inelastic) representing quark densities and photon spectrum [49].

6 Results and Discussion

6.1 Monopole-Antimonopole Annihilation

In Fig. 14 we show the total cross section for monopole-antimonopole production and the contribution from each of the individual processes described above as a function of

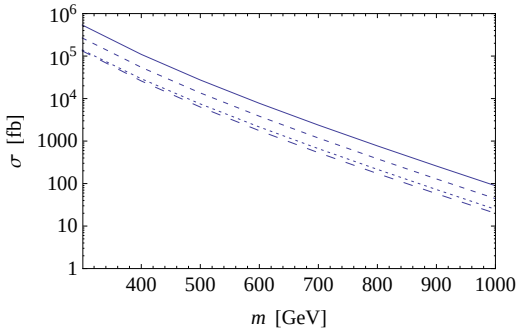

Figure 14: The total monopole-antimonopole production cross section (solid line) from $\gamma\,\gamma$ fusion in fb as a function of monopole mass. The different components of the cross section are shown: elastic (dotted line), semi-elastic (small dashed line) and inelastic (dashed line).

monopole mass. In order to set the mass axes we have taken into account the previous lower mass limit for the monopole of ref. [12] which was set at 360 GeV. The cross section is of $\mathcal{O}$(fb) thus we limit the high mass values to those potentially observable at present, or in the near future, by the LHC with an integrated luminosity of 5 fb^{-1}. Our result differs from that of ref. [26] around threshold.

We see in the previous figure that monopoles of mass around 500 GeV should be produced abundantly, while those of mass around 1000 GeV have a cross section which makes them difficult to detect in the near future, at least directly.

Since, as already mentioned, the LHC detectors have not been tuned to detect monopoles but are excellent detectors for γ's let us discuss next our annihilation cross section. In Fig. 15 we show the differential cross section for forward (solid) and right-angle (dotted) scattering given in fb/GeV as a function of the invariant mass of the $\gamma\,\gamma$ system. We have assumed a monopole of mass 750 GeV, chosen because the cross sections turned out to be close to the expected magnitude of the Higgs to $\gamma\ \gamma$ cross section above background. The cross sections are wide, almost gaussian, structures rising softly just above threshold (1500 GeV). LHC detectors are blind for forward scattering and have black spots due to construction features in the non-forward regions which do not allow for a full detection of photons. Therefore in order to obtain an educated estimation of the observable cross section we take the right-angle cross section and multiply it by 4π. This differential cross section is the smallest possible. However, away from threshold, it corresponds quite well to a realistic estimate, since, as we have seen, the elementary differential cross section drops fast with angle and moreover one should consider an efficiency factor for the various detectors.

In Fig. 16 we plot the right-angle differential cross section for the same monopole mass, showing the various contributions. The cross section features a wide distribu-

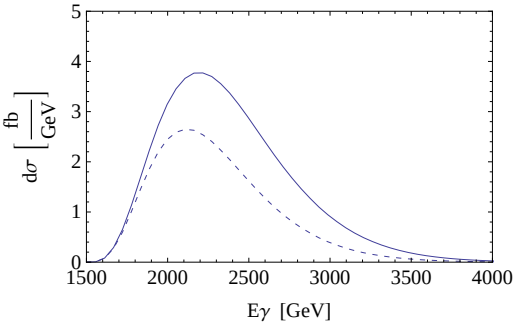

Figure 15: Forward (solid) and right-angle (dashed) cross sections for a monopole of mass 750 GeV.

tion, rising softly after threshold, 1500 GeV, and extending for almost 2000 GeV. The structure is centered about 2300 GeV. Clearly the soft rise of the differential cross section is a signature of the two-particle threshold, reminiscent of the β factor. The width of the structure is associated to the mathematical form of the box diagram, as can be seen for both electron-positron annihilation and monopole-antimonopole, from the form of the elementary cross section (Fig. 7).

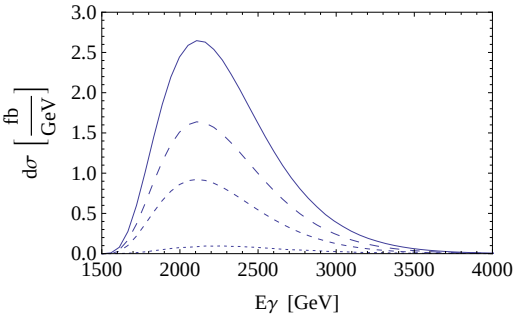

Figure 16: The right-angle scattering cross sections for a monopole mass of 750 GeV. The smallest is the inelastic cross section (dotted), next comes the elastic (dashed) and the biggest is the semi-elastic (long-dashed). The total cross section, the sum of the three, is represented by the solid curve.

In Fig. 17 we compare our total $\gamma\gamma$ cross section with that of the Higgs process obtained from ref. [54]. We have extrapolated their background to our energies using an inverse polynomial fit to their data and their exponential fit. Both procedures give a negligible background for the signals obtained with monopoles masses up to 1 TeV and even higher. In the left figure we translate the monopole-antimonopole threshold to the origin in order to compare the two signals. The Higgs signal above background

has been multiplied by 50 to make it visible. The figures correspond to a monopole of mass 750 GeV. It is clear from the curves that monopole-antimonopole annihilation should appear as a soft rise of the cross section above the background over a large energy interval. Actually the expected background from Standard Model processes is negligible in the kinematic region $E_{\gamma\gamma} \sim 1$ TeV. Hence the required selection criteria can be kept minimal, retaining thus the majority of the photon pairs produced in $m-\bar{m}$ annihilation in the analysis. Thus the search for monopole-antimonopole pairs will be practically background free at the LHC.

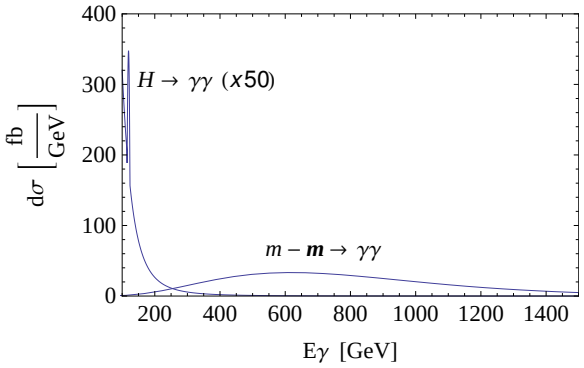

Figure 17: Comparison of the $\gamma\gamma$ monopole-antimonopole annihilation cross section for a monopole of mass 750 GeV with the Higgs $\gamma\gamma$ decay. The Higgs cross section above the background has been multiplied by 50. The monopole-antimonopole threshold has been set at the origin (100 GeV) (left).

Finally we study the mass dependence of the differential cross section. Fig. 18 is a LogLog plot of the cross section for three masses, $500, 750$ and 1000 GeV. In order to have a better comparison we have translated the thresholds to the origin. It is clear that the magnitude of the cross section and its extent falls rapidly with mass. For a low mass monopole, the magnitude of the differential cross section is of the order of ~ 1 pb/GeV, for an intermediate mass monopole the cross section is of the order of ~ 10 fb/GeV and for a heavy monopole is of the order of ~ 1 fb/GeV. If the monopole has a low mass, monopoles should be seen within the initial period of LHC running.

6.2 Monopolium Annihilation

Our aim is to show scenarios which could arise during the present LHC running period and to discuss general properties of the monopolium system which might serve when higher luminosities are achieved. In Fig. 19 we show the structure for the differential cross section. It is a wide bump, starting very close after threshold, i.e. the monopolium mass (1400 GeV in this case), and extending for about 1000 GeV . We show in the

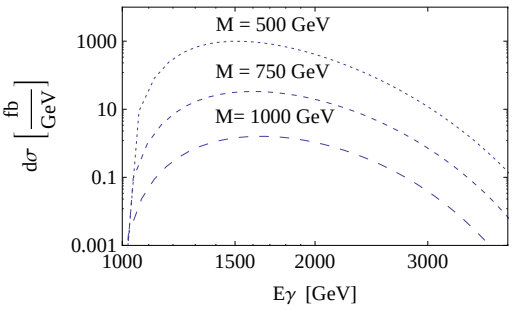

Figure 18: The cross section for monopole-antimonopole annihilation into $\gamma\gamma$ for three masses: 500 GeV (solid), 750 GeV dashed 1000 GeV (dotted).

figure the contribution of the different components to the cross section. The elastic and semi-elastic components dominate. The behavior is well understood by the structure of Eq. 12, the bump initiates due to the rising of the cross section close to threshold associated with its β behavior. Close to threshold β takes almost its asymptotic value of 1 and the $1/E$ behavior of the cross section starts to softly dominate (recall Fig. 12).

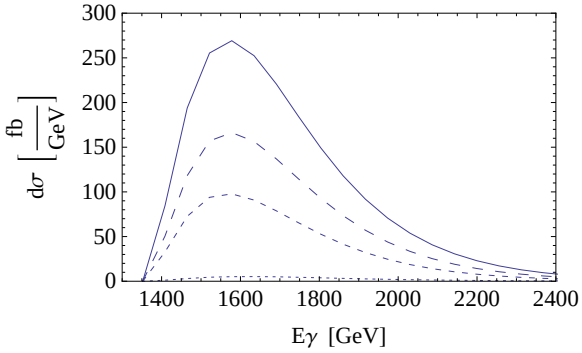

Figure 19: The differential cross section (solid line) and its components (semi-elastic (dashed), elastic (short-dashed) and inelastic (dotted)) as a function of the center-of-mass photon energy for a monopole mass of 750 GeV and a monopolium mass of 1400 GeV.

Two are the main physical dependences of the cross section: the monopole mass, m, and the monopolium mass, M. In Fig. 20 we fix the monopole mass to 750 GeV and vary the binding energy. We see that the cross section increases dramatically with binding energy. Thus the effect of the binding is twofold: it increases the cross section and it lowers the threshold from $2m$ the monopole-antimonopole production threshold. To observe the other dependence, in Fig. 21 we fix the binding energy to 100 GeV and

vary the monopole mass. The effect goes inversely proportional to the monopole mass, i.e., the lower the monopole mass the larger the cross sections.

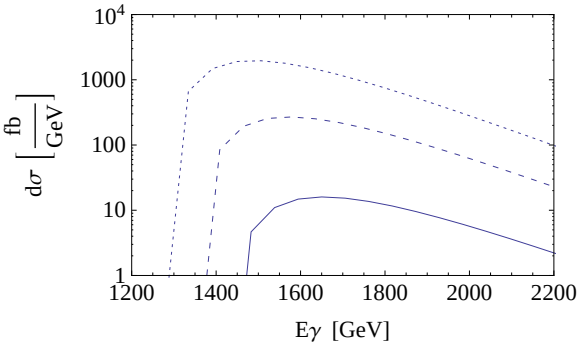

Figure 20: Differential two photon cross section as a function of the photon center-of-mass energy for a monopole mass of 750 GeV and different binding energies for monopolium: solid line 75 GeV, dashed 150 GeV and dotted 225 GeV.

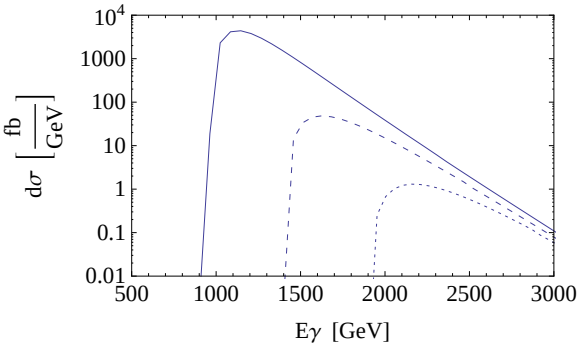

Figure 21: Differential cross section as a function of photon energy for different monopole masses: 500 GeV (solid), 750 GeV (dashed), 1000 GeV (dotted) and fixed binding energy (100 GeV).

We can summarize our findings by stating that low monopole masses and large bindings favor the detection of monopolium. Monopolium has the advantage over the monopole-antimonopole process of lowering the threshold, narrowing the bump and increasing the cross section with binding energy. In Fig. 22 we show three interesting effects, namely the two photon decays of Higgs, monopolium and monopole-antimonopole annihilation. The Higgs signal has been increased over the background by a factor of 50. The parameters for the monopolium cross section shown are $m = 750$ GeV and $M = 1400$ GeV, which have been chosen so that its signal is of the same size of that of

the monopole-antimonopole annihilation with a monopole mass of also 750 GeV. We note two of the features mentioned before, the lower threshold and the narrower bump structure. If we would increase the binding by a few tens of GeV the height of the bump would increase considerably with respect to the monopole-antimonopole cross section (recall Fig. 20). Note that the $\gamma\gamma$ conventional background at the monopole scenario in this kinematical region is extremely small, as measured recently by ATLAS in diphoton studies [55] and while searching for $H \to \gamma\gamma$ [56].

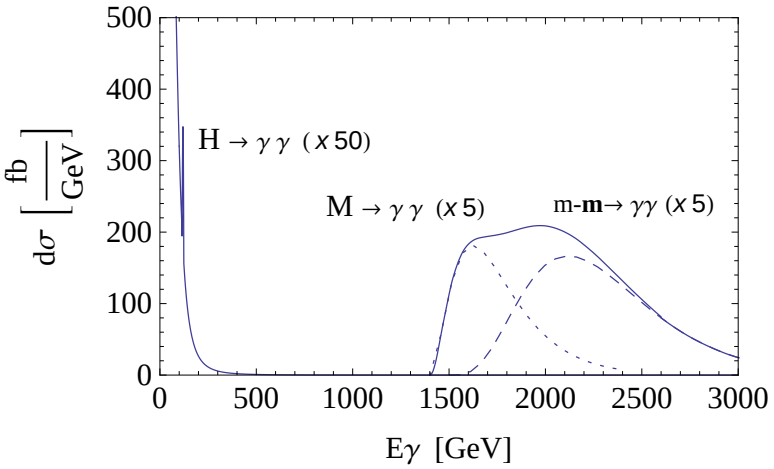

Figure 22: We show the differential two photon crossection with the Higgs signal (scaled by a factor of 50 over the background) where the monopolium and monopole-antimonopole contributions have been incorporated. We also show the monopolium signal (dotted) that presents a sudden rise at threshold, and the monopole- antimonopole (dashed) with a softer increase at threshold. Note that both signals were multiplied by 5 . The mass of the monopole in both cases is 750 GeV and that of the monopolium 1400 GeV. The background has been obtained from ref. [57].

If a broad bump would appear experimentally it could certainly arise from monopole dynamics. Thereafter the way to distinguish between the decay of monopolium and the annihilation of monopole-antimonopole would be through the angular dependence. In the present scenario, a spin zero monopolium, the angular decay properties would be similar to that of para-positronium [58], while that of monopole-antimonopole would be analogous to light-by-light scattering in QED [40, 43]. Moreover, the two pehenomena could occur simultaneausly, as happens in the case of electrons and positrons, where we have in light-by-light scattering electron-positron annihilation and positronium decay. If the latter were the case two bumps, if the overlap is not large, or a very broad flat bump, if the overlap is considerable, could be seen. The existence of one or two bumps depends very strongly on the binding dynamics and the monopole mass. Note that there is no possible confusion with the Higgs, since its width is narrow compared to

its mass. Moreover, the scattering cross section for a heavy Higgs in the two photon channel is extremely small compared to that in the other channels, and therefore, its characteristics would be known by the time a two photon bump would be seen.

7 Conclusions

The existence of Dirac monopoles would modify our understanding of QED. The DQC is a beautiful consequence of the existence of monopoles and therefore they represent an extremely appealing physical scenario. There is as of yet no experimental proof of their existence. This has led to approximate mass bounds which suggest a mass scale for the monopole above 500 GeV. LHC opens up this energy regime for research and therefore monopoles become again a subject of exciting experimental search.

The DQC, implying a huge magnetic coupling constant, complicates matters from the theoretical point of view. Non perturbative methods are required. We have avoided the problem by using an effective theory valid at one loop order. In our scheme, the effective coupling βg is still large away from threshold, but the expected high monopole masses provide a convenient cut-off which makes the theory meaningful. In the context of this theoretical scheme we are able to calculate monopole(antimonopole) production and monopole-antimonopole annihilation. Centering our description to LHC, a proton machine, we have described scenarios for the production of monopole-antimonopole pairs via photon fusion. We have described their annihilation into photons via the conventional box diagram, analogous to that of light-by-light scattering in conventional QED. The only difference in our approach is the introduction of a threshold factor in the form of a velocity. We have analyzed in detail the elementary process, light-by-light scattering at monopole energies, and have subsequently incorporated the description of the photon-photon elementary scattering into the initial proton-proton collision. One main assumption is that no other particle contributes to the box diagram in the region of interest. We have chosen in the present calculation a mass range which is above conventional particle masses and below the supersymmetric particle ranges. One could think of interference with elementary particle decays, however the latter would have a resonant structure which our box diagram does not have. Thus any interference would be avoided by their different geometric structure.

With all these preventions we have shown that monopoles up to 1 TeV in mass should be detected at LHC in the $\gamma\ \gamma$ channel at present running energies and with present luminosities. The signature is a rise of the cross section which should stay for a long energy range, because no resonant peak structure is to be expected.

Even if monopoles exist it might be possible that due to the very strong magnetic coupling they do not appear as free states but bound forming monopolium, a neutral state, very difficult to detect directly. We have analyzed the coupling of monopolium to photons and its contribution to light-by-light like scattering, i.e. monopolium's dy-

namical decay. We have found that for reasonable values of the monopole mass and relatively small, compared with their mass, binding energies, spin-zero monopolium disintegrates into two gammas with cross sections which are reachable with the currently available LHC integrated luminosity of 5 fb^{-1}.

Our investigations go beyond this wishful scenario. We have seen that the cross section depends both on the mass on the monopole and on that of monopolium, increasing inversely proportional to the monopole mass and being directly proportional to the binding energy. This means that similar cross section can be achieved with very heavy monopoles if the binding energy is large.

To conclude, without doubt, the appearance of a broad signal at threshold, in the two photon cross section, should be considered as a clear manifestation of the monopole presence. The implementation of our findings in detector analysis would provide actual observations.

Acknowledgement

We thank the authors of JaxoDraw for making drawing diagrams an easy task [59]. LNE, HF and CAGC were partially supported by CONICET and ANPCyT Argentina. VAM acknowledges support by the Spanish Ministry of Science and Innovation (MICINN) under the project FPA2009-13234-C04-01, by the Spanish Agency of International Cooperation for Development under the PCI projects A/023372/09 and A/030322/10 and by the CERN Corresponding Associate Programme. VV has been supported by HadronPhysics2, by MICINN (Spain) grants FPA2008-5004-E, FPA2010-21750-C02-01, AIC10-D-000598 and by GVPrometeo2009/129.

References

[1] P. A. M. Dirac, Proc. Roy. Soc. Lond. A **133** (1931) 60.

[2] J. D. Jackson, Classical Electrodynamics, de Gruyter, N.Y. (1982).

[3] N. Craigie, G. Giacomelli, W. Nahern and Q. Shafi, Theory and detection of magnetic monopoles in gauge theories, World Scientific, Singapore1986.

[4] P.D.B. Martin Collins, A.D. Martin and E.J. Squires, Particle Physics and Cosmology, Wiley, N.Y. (1989)

[5] B. Abbott *et al.* [D0 Collaboration], Phys. Rev. Lett. **81** (1998) 524 [arXiv:hep-ex/9803023].

[6] S. Eidelman *et al.* [Particle Data Group], Phys. Lett. B **592** (2004) 1.

[7] M. J. Mulhearn, "A Direct Search for Dirac Magnetic Monopoles," Ph.D. Thesis, Massachusetts Institue of Technology 2004, FERMILAB-THESIS-2004-51.

[8] G. Giacomelli and L. Patrizii, arXiv:hep-ex/0506014.

[9] A. Abulencia *et al.* [CDF Collaboration], Phys. Rev. Lett. **96** (2006) 201801 [arXiv:hep-ex/0509015].

[10] K. A. Milton, Rept. Prog. Phys. **69** (2006) 1637 [arXiv:hep-ex/0602040].

[11] W. M. Yao *et al.* [Particle Data Group], J. Phys. G **33** (2006) 1.

[12] A. Abulencia *et al.* [CDF Collaboration], Phys. Rev. Lett. **96** (2006) 011802 [arXiv:hep-ex/0508051].

[13] S. Balestra, G. Giacomelli, M. Giorgini, L. Patrizii, V. Popa, Z. Sahnoun and V. Togo, arXiv:1105.5587 [hep-ex].

[14] P. A. M. Dirac, Phys. Rev. **74** (1948) 817.

[15] Y. B. Zeldovich and M. Y. Khlopov, Phys. Lett. B **79** (1978) 239.

[16] C. T. Hill, Nucl. Phys. B **224** (1983) 469.

[17] V. K. Dubrovich, Grav. Cosmol. Suppl. **8N1** (2002) 122.

[18] L. N. Epele, H. Fanchiotti, C. A. Garcia Canal and V. Vento, Eur. Phys. J. C **56** (2008) 87 [arXiv:hep-ph/0701133].

[19] L. N. Epele, H. Fanchiotti, C. A. G. Canal and V. Vento, Eur. Phys. J. C **62** (2009) 587 [arXiv:0809.0272 [hep-ph]].

[20] I. F. Ginzburg, G. L. Kotkin, V. G. Serbo and V. I. Telnov, Nucl. Instrum. Meth. **205** (1983) 47.

[21] I. F. Ginzburg and S. L. Panfil, Sov. J. Nucl. Phys. **36** (1982) 850 [Yad. Fiz. **36** (1982) 1461].

[22] Yu. Kurochkin, I. Satsunkevich, D. Shoukavy, N. Rusakovich and Yu. Kulchitsky, Mod. Phys. Lett. A **21** (2006) 2873.

[23] I. F. Ginzburg and A. Schiller, Phys. Rev. D **57** (1998) 6599 [arXiv:hep-ph/9802310].

[24] I. F. Ginzburg and A. Schiller, Phys. Rev. D **60** (1999) 075016 [arXiv:hep-ph/9903314].

[25] G. R. Kalbfleisch, K. A. Milton, M. G. Strauss, L. P. Gamberg, E. H. Smith and W. Luo, Phys. Rev. Lett. **85** (2000) 5292 [arXiv:hep-ex/0005005].

[26] T. Dougall and S. D. Wick, Eur. Phys. J. A **39** (2009) 213 [arXiv:0706.1042 [hep-ph]].

[27] G. Aad *et al.* [ATLAS Collaboration], JINST **3** (2008) S08003.

[28] R. Adolphi *et al.* [CMS Collaboration], JINST **3** (2008) S08004.

[29] J. L. Pinfold, AIP Conf. Proc. **1304** (2010) 234; J. L. Pinfold [MOEDAL Collaboration], CERN Cour. **50N4** (2010) 19.

[30] L. N. Epele, H. Fanchiotti, C. A. G. Canal, V. A. Mitsou and V. Vento, arXiv:1104.0218 [hep-ph].

[31] L. N. Epele, H. Fanchiotti, C. A. Garcia-Canal, V. A. Mitsou and V. Vento, arXiv:1107.3684 [hep-ph].

[32] J. S. Schwinger, Phys. Rev. **144** (1966) 1087.

[33] D. Zwanziger, Phys. Rev. D **3** (1971) 880.

[34] L. P. Gamberg and K. A. Milton, Phys. Rev. D **61** (2000) 075013 [arXiv:hep-ph/9910526].

[35] L. F. Urrutia, Phys. Rev. D **18** (1978) 3031.

[36] J. M. Cornwall, Phys. Rev. D **26**, 1453 (1982).

[37] S. Weinberg, Physica A **96** (1979) 327.

[38] C. Itzykson and J. B. Zuber, *New York, USA: McGraw-Hill (1980) 705 P.(International Series In Pure and Applied Physics)*

[39] R. Karplus and M. Neuman, Phys. Rev. **80** (1950) 380.

[40] R. Karplus and M. Neuman, Phys. Rev. **83** (1951) 776.

[41] H. Euler Ann. Phys. **26** (1936) 398.

[42] A. Achieser, Physik Z. Sowjetunion **11** (1937) 263.

[43] P. L. Csonka and K. S. Koelbig, Phys. Rev. D **10** (1974) 251.

[44] J.M. Jauch and F. Rorhlich, The theory of electrons and photons (Springer 1975).

[45] M.E. Peskin and D.V. Schroeder, An introduction to quantum field theory, (HarperCollins, 1995).

[46] B. C. Allanach, K. Odagiri, M. A. Parker and B. R. Webber, JHEP **0009** (2000) 019 [arXiv:hep-ph/0006114].

[47] M. R. Pennington, Acta Phys. Polon. B **37** (2006) 857 [arXiv:hep-ph/0511146].

[48] K. A. Milton, arXiv:0802.2569 [hep-ph].

[49] M. Drees, R. M. Godbole, M. Nowakowski and S. D. Rindani, Phys. Rev. D **50** (1994) 2335 [arXiv:hep-ph/9403368].

[50] The Cteq6 parton distribution functions can be found at [http://www.phys.psu.edu//cteq/].

[51] E. J. Williams, Phys. Rev. **45** (1934) 729.

[52] C. F. von Weizsacker, Z. Phys. **88** (1934) 612.

[53] M. Drees and D. Zeppenfeld, Phys. Rev. D **39** (1989) 2536.

[54] G. Aad *et al.* [Atlas Collaboration], Phys. Rev. Lett. **106** (2011) 121803 arXiv:1012.4272 [hep-ex].

[55] G. Aad *et al.* [ATLAS Collaboration], arXiv:1107.0581 [hep-ex].

[56] ATLAS Collaboration, "Search for the Higgs Boson in the Diphoton Channel with the ATLAS Detector using 209 pb^{-1} of 7 TeV Data taken in 2011," ATLAS Note, ATLASCONF- 2011-085 (2011).

[57] ATLAS Collaboration, "ATLAS Sensitivity Prospects for Higgs Boson Production at the LHC Running at 7 TeV," ATLAS Note, ATL-PHYS-PUB-2010-009 (2010).

[58] G. S. Adkins, R. N. Fell and J. Sapirstein, Phys. Rev. A **63** (2001) 032511.

[59] D. Binosi and L. Theussl, Comput. Phys. Commun. **161** (2004) 76 [arXiv:hep-ph/0309015].